Module 4: Interferometry

Lecture 21: Applications - buoyant convection

The Lecture Contains:

Previous Next

APPLICATIONS

Three sets of experiments involving (1) buoyant flow around a protruding heater [77], (2) transient convection in a square cavity a differentially heated fluid layer are discussed in the present section. All of them employ interferometry, to thermal convection.

Buoyancy- Driven Flow around a Protruding Heater

Buoyancy-driven flow in the vicinity of a protruding heated block copper block placed on a vertical wall and exposed to the ambient is experimentally studies here. The copper block is of height h, protrusion b, and a length L, which is much larger than h and b. it is located on a vertical Bakelite board with its longest dimension L lying in the horizontal plane. All measurements have been carried out at steady state. The average Nusselt number as a function of Rayleigh number has been reported in this work. The thermal wake above the block as visualized by the Mach-Zehnder interferometer is also presented in this study.

The problem addressed here arises frequently in the thermal design of high-performance electronic components such as integrated chips in computers. An overall review of the subject for practical cooling configurations of electronic circuit boards has been presented by Incropera [103]. Heat transfer from arrays of protruding three-dimensional heaters under forced flow conditions have been experimentally studies by Garimella and Eibeck [104]. Experiments on two-and three- dimensional natural convection heat transfer form vertical, discrete, and arrays of flush and mildly protruding heaters have been presented in the literature [105]. Nusselt number and wake size in natural convection for vertical and horizontal protruding thermal sources using thermocouple data have been studies by Kang and Jaluria [106].

The dimensionless parameters of the problem are the aspect ratio $A(=h/b)$, Rayleigh number (Ra) and the average Nusselt number (Nu) based on the height h of the copper block. Fluid properties are evaluated at the average of the heater and room temperatures. There is some uncertainly in the form of the boundary condition at the heater surface since it can be prescribed as constant temperature or as constant heat flux. The use of a copper block would suggest the former, but since the heater size is quite small in the present study we continue to examine the constant heat flux boundary condition. The respective values of the temperature difference in the definitions if Ra and Nu are computed as $(T_c - T_{\text{room}})$ and $(q(h+2b)/k)$ respectively. In all the data presented in this work, the aspect ratio A is equal to two.

Two different heaters of sizes $(h, b, L,) = (10, 5, 192)$ mm and $(16, 8, 180)$ mm have been employed in the present work. Surface temperatures employed are vary from $60°C\ to\ 101°C$ are in the range of $23.7 - 25.6°C$.. The copper block is electrically powered by a nichrome-wound heater placed behind it. The electrical resistance of the nichrome wire used is 95 ohms/m. the voltage applied to the heater is stabilized using a series of variances. The entire heater assembly is mounted on a bakelite sheet (Fig.29). This sheet is placed vertically in an enclosed test cell that straightens the flow approaching the copper block.

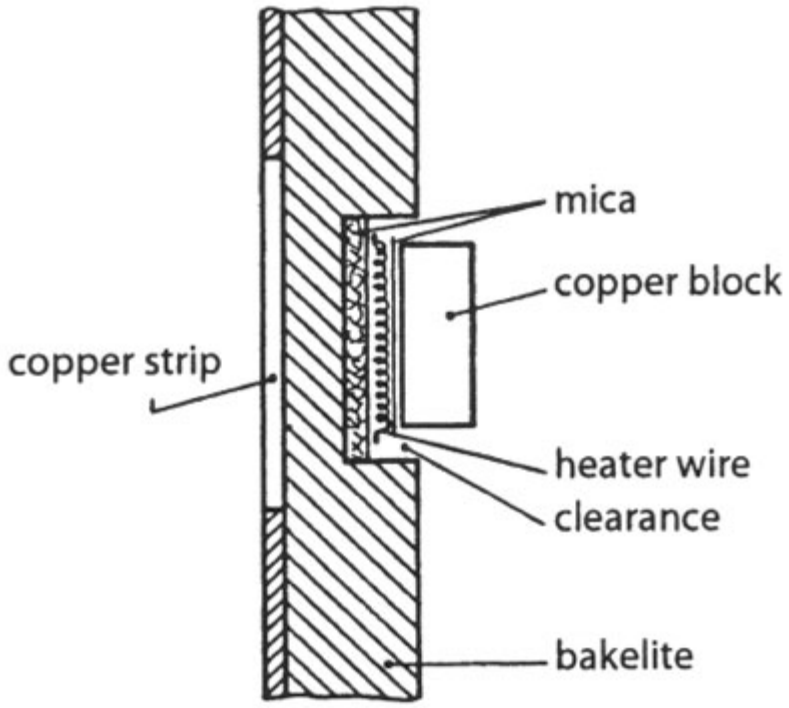

Figure 4.35: Schematic of the experimental apparatus of a protruding heater

Previous Next

Heat transfer from the electric heater to the ambient from the rear side of the test cell is estimated as follows. A thin copper strip of 25 mm height is firmly held against the Bakelite sheet and its temperature is monitored by an array of thermocouples. The energy lost to the ambient outside the test cell is obtained by applying vertical flat plate correlations of natural convection to the copper strip. The ambient energy loss is found to be about 10% of the electrical input. Radiation losses are found to be negligible for the smaller of the copper blocks since its area is small and the surface is polished. For the larger block, radiation accounts for up to 5% of the energy input. It has been accounted for through detailed calculations including shape factors. Energy transferred in a direction parallel to the gravity vector to the Bakelite sheet supporting the copper block is not considered as a loss since it is recovered by the fluid ahead and beyond the heater.

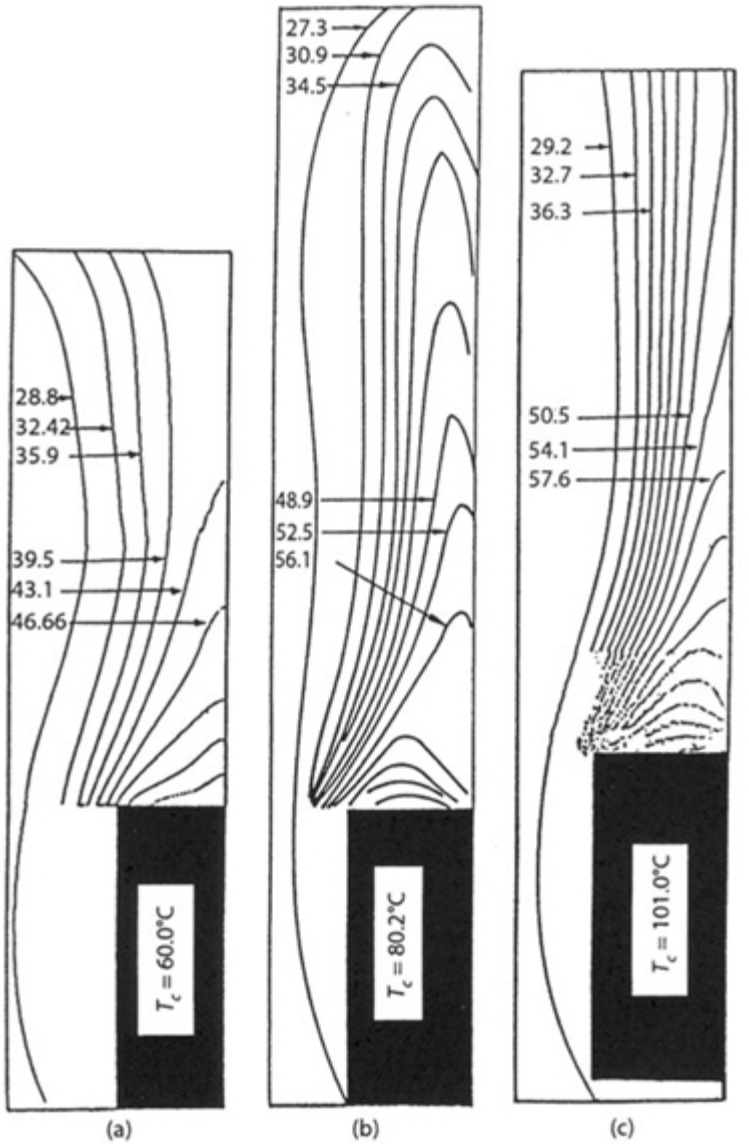

Figure 4.36: Thinned interferometric fringe patterns around a protruding heater on a vertical surface.

The thermal field in the vicinity of the heater has been studies using Mach- Zehnder interferometer. The path of the light beam is arranged to be parallel to the heater length. The interferograms are

collected in the infinite fringe setting and hence the fringes are isotherms. Skeletonized fringes alone have been presented here. The fringe density near the chip is high and is corrupted by refraction errors. Hence the near-wall fringes have been removed using image processing operations. The outer most fringes representing the thermal boundary layer and all the fringes in the wake have been preserved. For the experiments reported here the temperature drop per fringe shift is 3.5 K.

Previous Next

Interferograms

Interferometric data for the smaller copper block of height 10 mm and a protrusion of 5 mm is presented first. Figure 4.36 shows thinned fringes in the proximity of the heater at temperatures of $60°, 80.2°,$ and $101°C$. Since the fluid below the lower surface is nearly stationary, fringes in this region have not been shown. The images have been recorded with varying magnifications to maintain clarity. The outermost fringe can be treated as the edge of the boundary- layer thickness can, however, be used for analysis. For an assumed quadratic temperature as well as constant heat flux boundary conditions is $2h/\delta$.

An examination of figure 4.36 shows the following trends. With temperature increasing from $60°C$ to $80.2°C$ the thermal boundary-layer thickness decreases. Further increase in temperature to $101°C$ does not lead to any significant reduction in the boundary-layer thickness. At $60°C$, the boundary-layer thickness is nonzero at the leading edge of the heated block. For the other two temperatures, δ is small at this location.

A drop in the value of boundary layer thickness indicates an increase in the local Nusselt number. Hence the Nusselt number on the vertical face increase as one goes from $60°C$ to $80.2°C$. This increase is only marginal between $80.2°C$ and $101°C$, the fringe density, and hence, heat flux over the upper horizontal face, continually increases as one move from $60°C$ *to* $101°C$. This is also a source of increasing the average Nusselt number with clip temperature.

Previous Next

Heat Transfer Rates

Figure 4.37 shows a plot of the local Nusselt number on the vertical face of the copper block determined using the boundary- layer thickness. The average values of the Nusselt number on the vertical face $(= \mathrm{Nu}(v))$, and Nusselt number at the midpoint of the chip $(= \mathrm{Nu}(m))$ corresponding to the three Rayleigh numbers are given in Table 6. Except for a block temperature of $60°\mathrm{C}$, these are larger than the corresponding average for the entire heater. At $T_c = 60°\mathrm{C}$, the boundary- layer thickness at the leading edge is nonzero, resulting in a low Nusselt number over the vertical face of the copper block.

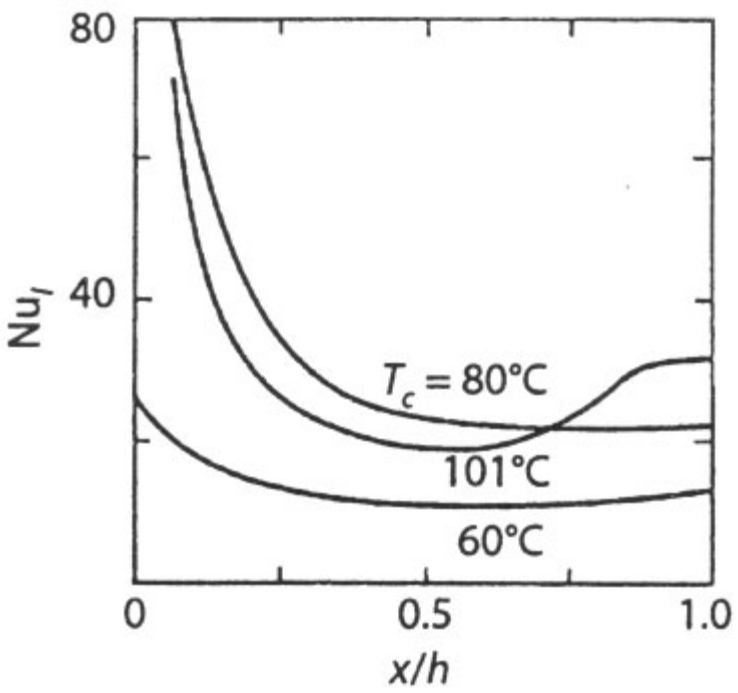

Figure 4.37: Local Nusselt number as a function of distance along the copper block.

Table 6: Average and Midpoint Nusselt Numbers an the Vertical Face of the Copper Block

T_c, °C	60	80.2	101
$\mathrm{Ra}(T)$	2477	3349	3894
$\mathrm{Nu}(v)$	13.5	30.8	28.6
$\mathrm{Nu}(m)$	10.5	23.0	19.0

Previous Next

Table 7 gives values of Nusselt number (Nu) as a function of the Rayleigh number $(\mathrm{Ra}(T)$ and $\mathrm{Ra}(q))$ based on the average heat transfer measurements of the present study.

It is of interest to compare the result obtained in Table 7 with correlations and data available in the literature. This comparison for buoyancy- driven flows from flush as well as protruding surfaces is presented below.

Isothermal vertical flat plate

$$\mathrm{Nu} = \left(0.825 + 0.387F(\mathrm{Pr})\left(\mathrm{Ra}(T)\right)^{1/6}\right)^2$$

where $F(\mathrm{Pr}) = \left(1 + (0.492/\mathrm{Pr})^{9/16}\right)^{-8/27}$. The minimum and the maximum Nusselt numbers computed using this equation for the limiting Rayleigh numbers in table 7 are 4.07 and 6.11, respectively.

Constant heat flux vertical surface

$$\mathrm{Nu} = 1.2\mathrm{G}(\mathrm{Pr})^{0.2}\mathrm{Ra}(q)^{0.2}$$

where $G(\mathrm{Pr}) = \mathrm{Pr}/(4 + 9\mathrm{Pe}^{0.5} + 10\mathrm{Pr})$. The minimum and maximum Nusselt numbers from this correlation are 5.28 and 7.86, respectively.

Protruding block on a vertical surface, aspect ratio=2.5,

For $1 \times 10^6 < Ra(q) < 4 \times 10^6$, Nu varies from 10 to 12.

Fully developed flow foe an array of protruding blocks, aspect ratio = 2

For $10^3 < \mathrm{Ra}(T) < 10^4$, Nu varies from 5 to 8.

Cuboid Models for an isothermal block of dimensions $H \times B \times L$, $\mathrm{Ra}(T) < 10^{11}$.

Table 7: Average Nusselt Number as a Function of Rayleigh Number; $(Ra(T) \geq 9290$ *corresponds to the larger block*$)$

$Ra \times 10^{-3}$	2.48	3.35	389	9.29	13.3	14.9	17.3
$Ra \times 10^{-4}$	8.7	12.7	15.1	28.7	44.3	53.0	63.6
Nu	13.2	13.5	13.8	14.7	16.0	17.1	17.6

Previous Next

$$\mathrm{Nu} = \mathrm{Nu}_c + F(\mathrm{Pr})G\mathrm{Ra}^{0.25}$$

where

$$\mathrm{Nu}_c = \frac{3.192 + 1.868\left(\frac{L}{H}\right)^{0.25}}{\left(1 + 1.189\frac{L}{H}\right)^{0.5}}$$

$$G = 2^{1/8}\left(\frac{H(L+B)^2}{\left(LB + H(L+B)\right)^{1.5}}\right)^{0.25}$$

$$F(\mathrm{Pr}) = \frac{0.67}{\left(1 + \left(\frac{0.5}{\mathrm{Pr}}\right)^{9/16}\right)^{4/9}}$$

For the range of Rayleigh numbers given in Table 7, this equation gives Nusselt numbers in the range of 4.75 to 7.45.

The qualitative agreement of the local Nusselt numbers of the present study with is good. Discrepancies are possible in the average Nusselt number since these authors use thermocouples to determine the local Nusslet number. Resulting in loss of resolution, especially near the peak values. It is clear that the flush heater correlations substantially underpredict the average Nusselt number. As discussed by Park and Bergles [105], this discrepancy is due to the inapplicability of large plate correlations for short segments, especially near the leading edge. Conduction losses to the supporting plate are significant for small surfaces and lead to a higher measured Nusselt number. The cuboid model also underpredicts the Nussselt number because it is primarily designed for a fin assembly and not an isolated copper block. The Nusselt number for a block located in an array is smaller than for a single block since the fluid approaching the block is preheated and the thermal boundary-layer over the vertical face is thick. For the isolated heated surface considered in the present work, the boundary- layer thickness (Figure 4.38) is zero at the leading edge and at all Rayleigh numbers except the lowest value.

Closure

Heat transfer in natural convection from an isolated protruding heater is found to be larger than that computed from correlations for a flush heater, a large cuboid, and data for an array of blocks. Interferometric study shoes the local Nusselt number over the vertical face of the copper block to be quite large. This factor along with conduction to the supporting plate in the direction provides the reasons for this difference.

Previous Next

Transient Convection in a Two- Dimensional Square Cavity

An interferometric study of transient natural convection in a long air-filled square cavity is reported. The top and bottom walls of the cavity are maintained at uniform temperatures at all times in an unstably stratified configuration. Three different Rayleigh numbers namely $8.79 \times 10^4, 1.98 \times 10^5$ and 3.38×10^5 have been considered. The orientation of the light beam is maintained parallel to the longest dimension of the cavity. The fringes thus obtained reveal depth-averaged isotherm patterns in the cavity at various instants of time. The image is filtered and the fringes are thinned using image processing operations. Subsequently, the local and average heat transfer parameters in t he experimental setup have been computed. Results of the present study of show that the onset of flow in the cavity is bicellular. However, the flow is unicellular for the most part of the transient. The flow becomes increasingly vigorous with time and the average Nusselt number of the cavity is a maximum at steady state.

Buouancy- driven flow in an air-filled cavity heated from below is a problem of fundamental as well as practical importance. A summary of experimental and theoretical result including several correlations for buoyancy-dominated flow is presently available [89]. These results pertain essentially to steady-state situations, with only a few numerical results being available for transient convection. One of the principal difficulties associated with transient flows is the measurement of the wall heat flux. Energy balance methods require careful accounting of losses and are simple to use only after steady state has been reached. In contrast to this, optical methods of measurement have several advantages. These include non-intrusiveness, absence of inertia while following transient, and the ability of a light beam to scan a flow field rather than the flow property at a point. Besides they can be used for qualitative as well as quantitative analysis of the problem at hand since the fringe spacing or the fringe thickness, however, places a lower limit on the length scales that can be resolved by the image.

Interferometric study of natural convection in a two-dimension cavity whose side walls are heated has been reported earlier [108]. A similar study for a horizontal cylindrical annulus has also been described [109]. The study that comes closest to the present work is that of Eckert and Carlson [110] where the effect of wall conduction on natural convection in a square cavity has been presented using interferometry. The bottom-heated/top-cooled configurations is one of the several arrangements considered in Eckert and Carlson [110]. Features such as plume formation and fringe symmetry about the vertical plane have been observed and these are similar to the results obtained in the present work. However, there are significant differences arising from initial and boundary conditions and in the data reduction procedures.

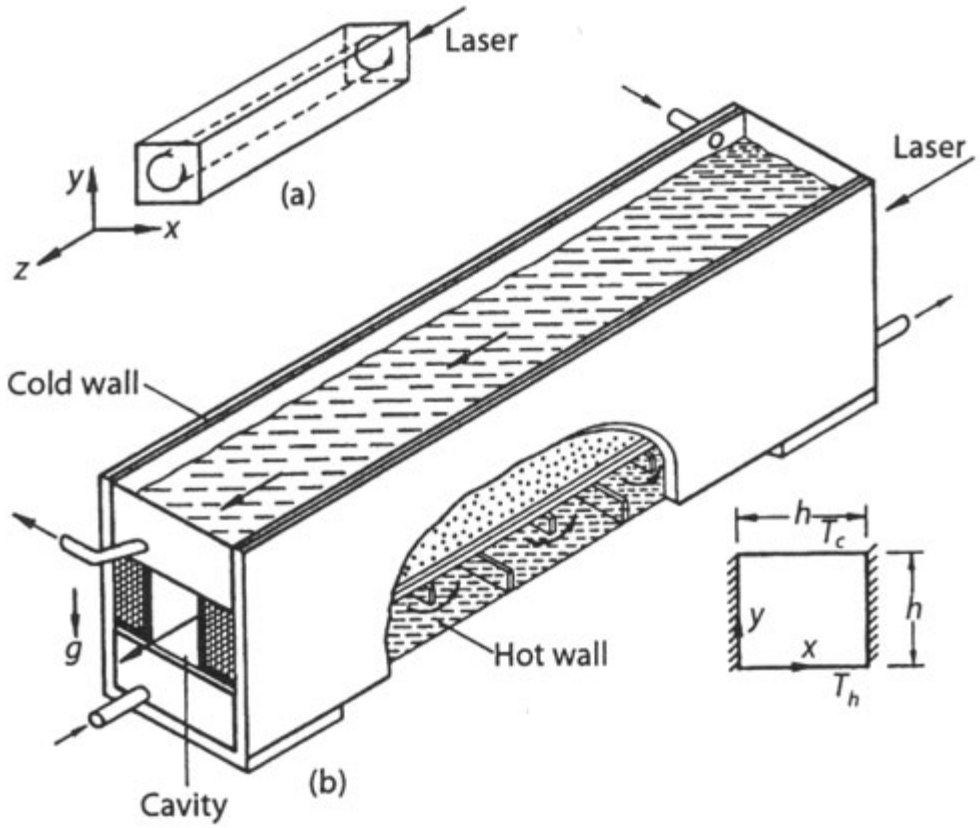

Figure 4.38: (a) Flow patterns in an infinite fluid layer and a square cavity; (b) schematic of the test cell.

more...

Previous Next

Steady state

Results are presented below for three Rayleigh number namely $8.79 \times 10^3, 1.98 \times 10^4$ and 3.38×10^4, and corresponding to cavity sizes of 4.0, 5.0, and 5.7 cm respectively. Figure 4.43 (a) shows the overall distribution of fringes in the full cavity at steady state attained with a Rayleigh number of 8.79×10^3. The spacing among fringes near the wall is seen to be small around the midplane of the cavity and gradually increases towards its edges. Since each fringe is an isotherm a small fringe spacing gives rise to a large local heat flux. The largest local heat flux on the cavity walls at steady state occurs around the midplane of the cavity. The fluid accelerates on one side of the midplane, reaches a maximum at this point, and decelerates to small values on the other side of the cavity, as it approaches the side walls. The overall flow pattern in the cavity is hence unicellular.

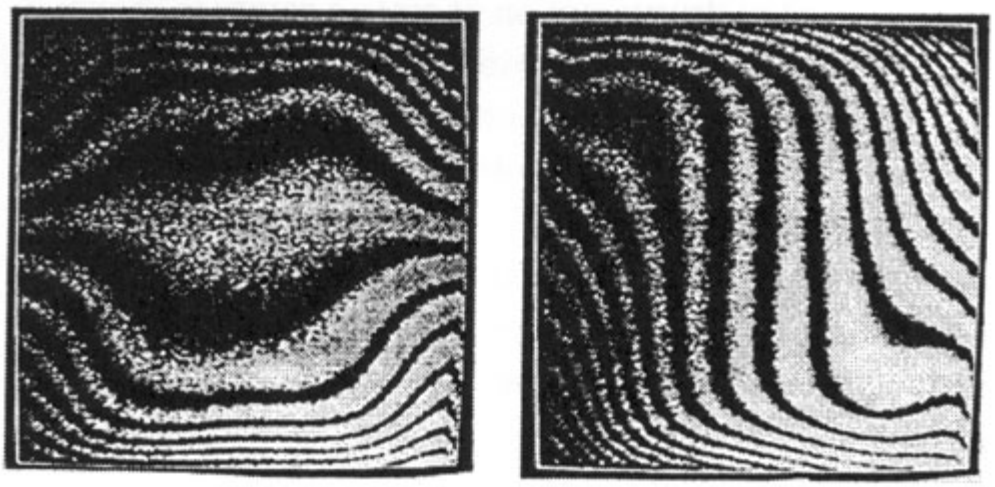

Figure 4.43: (a) Fringe patterns at steady state in a square cavity; (b) wedge fringes at steady state in a square cavity Fo = 50

Figure 4.43 (b) shows wedge fringes in the cavity at steady state at the same Rayleigh number of 8.79×10^3. The wedge fringes are obtained by deliberately misaligning the mirrors of the interferometer so that under zero flow conditions a set of parallel fringes are seen. When temperature gradients are present in the test cell the fringes are curved and the fringe slope is a measure of the local heat flux. The direction in which the fringes are displaced depends on the direction to the local fluid velocity. Figure 4.43 (b) shows that the fringes are displaced to the right near the bottom wall and to the left near the top wall. This confirms the result from the infinite fringe setting (fig.4.43 (a) that the flow in the cavity is unicellular with roll moving in an anticlockwise direction.

Previous Next

The intrinsic symmetry of the cavity and associated boundary conditions affords the formation of many cells whose axes are parallel to the cavity length. A single cell is preferred over other configurations owing to several factors that include mild imperfections in the experimental apparatus. A qualitative explanation can be given in terms of the energy requirement to sustain multicellular flow. In a square cross-section and at modaerate Rayleigh numbers, one can expect unicellular flow to consume the least energy and hence be most likely to appear in the cavity. The present set of experiments, however, provide evidence of bicellular flow for small-time and is discussed in the following sections

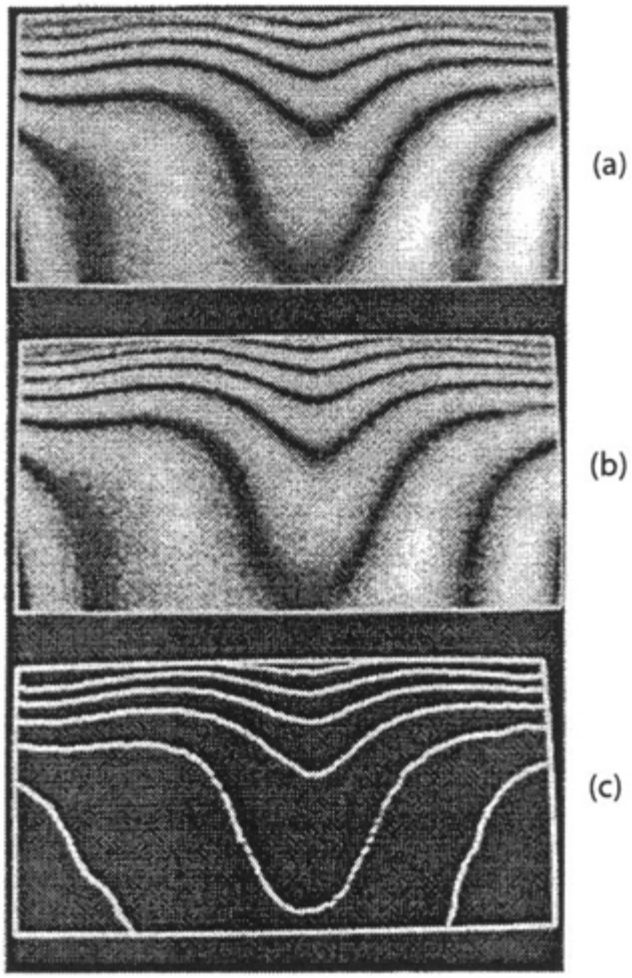

Figure 4.44: Fringes near the cold wall during transient convection. (a) Original, (b) Fourier-filtered and (c) Fringe-extracted Image, $Ra < 10^6$

Previous Next

Evolution of the Flow Field

Figure 4.44 (a-c) respectively show the original fringe pattern, the fourier-filtered image and, the fringe skeleton extracted using the procedure given earlier. The figure represents fringe patterns in the vicinity of the cold upper wall during the transient period at a Rayleigh number of figure 4.44 (a-c) and a Fourier number of 6.34. Figures show the original and the processed fringes near the cold wall for the same Rayleigh number at a Fourier number of 91.26. The near-wall fringes are nearly stationary at this time and steady state can be assumed to have been reached.
The interferograms shows above have been obtained at the infinite fringe setting and hence fringes are coincident with isotherms. At the center of the cold wall, the isotherms in Figure 4.44 are straight and hence correspond to parallel flow. A displacement of the isotherms is indicative of transverse flow. This is seen near the side walls in Figure 4.44 where flow moves up and down in the vertical direction to complete a loop. Displacement of the isotherms is also seen at the center of the cavity in figure 4.44. This is proof of the existence of two convection cells during the early stages of evolution of fluid movement.

Heat Transfer

Table 8 compares the average Nusselt number computed in the present work at the end of three hours with the steady state correlation given in Gebhart al. [89]. This correlation is applicable for a rectangular cavity with a moderate aspect ratio, but is independent of the aspect ratio itself. It is given as

$$\mathrm{Nu} = 1 + 1.44\left[1 - \frac{1708}{\mathrm{Ra}}\right] + \left[\left(\frac{\mathrm{Ra}}{5830}\right)^{1/3} - 1\right] \qquad (16)$$

for $Ra < 10^6$. The variation of the Nusselt number for each half of the cavity and for the cavity as a whole as a function of time are given in Table 9. A study of the transient data reveals the following features. For a given Rayleigh number, the average Nusselt number in the cavity is a maximum as steady state is reached. This is quite consistent with the fact that the flow (measured in terms of the maximum velocity or minimum stream function) is initially quiescent and increasingly becomes vigorous with the passage of time.

Table 8: Average Steady State Nusselt Number in a Square Cavity

$Ra \times 10^{-4}$	Nu (present)	Nu [89]	% difference
8.79	3.56	3.89	8.5
19.8	4.35	4.67	6.9
33.8	5.07	5.30	4.3

Previous Next

Table 9: Average Nusselt Number as a Function of Fourier Number

$Ra = 8.79 \times 10^4$				
Fo	6.34	11.5	35.7	91.3
Nu (left)	2.21	3.42	3.65	3.45
Nu (right)	2.06	3.11	2.45	3.68
Nu (cavity)	2.13	3.26	3.06	3.56
$Ra = 1.98 \times 10^5$				
Fo	9.14	13.7	20.3	60.94
Nu (left)	2.24	2.52	4.53	4.89
Nu (right)	2.64	2.79	3.77	3.81
Nu (cavity)	2.44	2.66	4.15	4.35
$Ra = 3.38 \times 10^5$				
Fo	8.93	31.9	47.4	65.7
Nu (left)	2.87	4.47	4.54	5.89
Nu (right)	3.33	4.49	4.31	4.26
Nu (cavity)	3.1	4.48	4.42	5.07

The increase in Nusselt number is however not found to be monotonic. The thermal field is seen to be symmetric with respect to the vertical axis dividing the cavity only at the lowest Rayleigh number (Ra=8.79 x 10^3). It is not symmetric at higher Rayleigh numbers, both during the transient as well as steady state. This is also seen in the average Nusselt numbers obtained for each half of the cavity. Hence, analyses that assume symmetry are likely to yield incorrect results.

Previous Next

Table 9 shows that at any Rayleigh number the initial increase in Nusselt number is rapid. This is followed by a slow transient until steady state is reached. This behavior can be explained as follows. The initial increase in Nu is controlled by the formation of boundary-layers near the hot and cold walls and the characterstic distance is this boundary layer thickness. Hence, the characterstic time over which initial changes in Nu are significant is quite small. At larger times heat transfer is established across the cavity dimension and the chnges in Nu occur at slower rate.

For all three Rayleigh numbers studied, the initial fringe patterns are qualitatively identical to those shown in Figure 4.44 (a). the fringes in this figure shoe a thick boundary- layer and a plume descending downwards along the vertical axis of the cavity. This suggests that the flow is initially bicellular. At later times the flow pattern reverts to a unicellular form with nearly constant boundary-layer thickness over the horizontal cavity walls (Fig. 4.45(a)). There is a considerable amount of uncertainty in the exact time instant at which this transition occurs. It corresponds approximately to a Fourier number of 10 while steady state is reached at around $Ra = 8.79 \times 10^3, 1.98 \times 10^4 \text{ and } 3.38 \times 10^4$. Once the flow becomes unicellular, transients are characterized by the formation of newer fringes. This represents the penetration of the thermal front into the bulk of the fluid. The process continues until steady state is reached.

Figure 4.36 (a-c) show the local Nusselt number at the cold wall of the cavity at $Ra = 8.79 \times 10^3, 1.98 \times 10^4 \text{ and } 3.38 \times 10^4$ respectively. Transient as well as steady state distributions are shown in these figures. The corner regions of the cavity are zones of high heat transfer and this is seen as spikes in the distribution of the local Nusselt number. These distributions show a minimum in the local Nusselt number at the midpoint of the cavity walls during the early transient. As stated above, this corresponds to the formation of two convection cells in the test call. In contrast, the local Nusselt number reaches a maximum around the same point at steady state. The local values of the Nusselt number differ considerably from their average computed over the mathematical definition of an average. An average based on Simpson's rule has been used in present work.

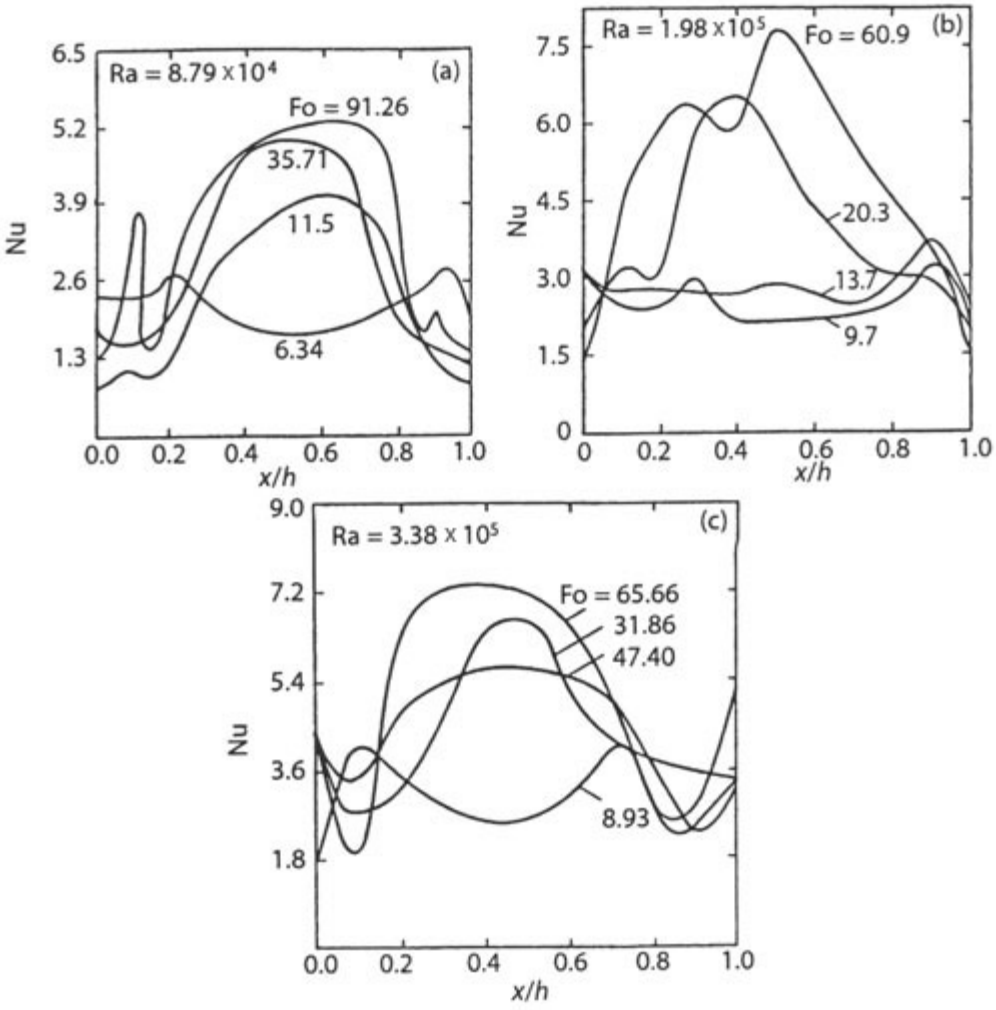

Figure 4.45: Local Nusselt number as a function of distance and time $Ra = 8.79 \times 10^3, 1.98 \times 10^4$ and 3.38×10^4

Closure

Transient Rayleigh-Benard convection in a square cavity with rigid walls has been experimentally studied. Results show that the time-evolution of flow is initially bicellular, while it is unicellular at steady state. The sense of unicellular motion depends on the experimental bias. Experiments also show a large variation with distance in the local Nusselt number at the cold wall. The evolving flow shows symmetry at the lowest Rayleigh number studied. Symmetry is however lost when the Rayleigh number is increased. The average cavity Nusselt number reaches a maximum at steady state.

Previous Next

The present work is concerned with visualizing isotherms in square cavity at various instants of time. The top and bottom walls of the cavity are respectively cold and hot and their temperatures are maintained constant for all time. This is the classical Rayleigh-Benard problem with confining side walls. The original problem of convection in an infinite fluid layer of small thickness admits three-dimensional cellular flow as solution. This is, however, considerably modified in the presences of confining side walls [111, 112] and at higher Rayleigh numbers. The formation of longitudinal rolls with their axes aligned normal to the shortest side has been observed in experiments on a horizontal fluid layer [41]. It is to be expected that when symmetry planes between adjacent cells are replaced by adiabatic walls. There will be no fundamental change in the flow pattern. This assumption has also been made implicitly in Tolpadi and Kuehn [8]. Fluid contained in the cavity whose vertical cross-section is a square and is long in the third dimension in the horizontal plane, is thus expected to exhibit cellular motion with the cell axis parallel to the longest side (Figure: 4.38(a)). If the length exceeds a critical value, two cells with the same direction of vorticity appear in the cavity. Since the cells are unidirectional, the temperature distribution within the two cells is similar. Hence the average temperature distribution obtained by optical projection is representative of the flow field at any section along the cavity length.

Interferograms have been obtained in the present work by orienting the light beam parallel to the longest dimension of the cavity. Rayleigh numbers considered in the study are $8.79 \times 10^4, 1.98 \times 10^5$ and 3.38×10^5 . These are large in comparison to the critical Rayleigh number for the infinite fluid layer. These are, however, close to the critical value for a cavity with confining side walls [113]. Fringe pattern have been thinned using image processing operations. The thinned fringes near the cold wall have been used to compute the local Nusselt number. Images have been acquired during the transient evolution of the thermal field as well as at steady state. The images show distinct flow patterns during the early transient phase in comparison to steady state.

The apparatus used to study buoyancy–driven motion of air in a cavity is shown in Figure 4.38(b). the cavity is of a square cross-section with its width and height being adjustable in the range of 4 to 6 cm.The top wall is cooled with the help of chilled water from a constant temperature bath to a temperature of around $10^{\circ}C$, while the bottom wall is maintained at a temperature of around $25^{\circ}C$, (close to room temperature). The temperatures of both the walls are maintained constant for the entire duration of the experiment. In the present study, special precautions have been taken so the top and bottom walls are maintained constant for the entire duration of the experiment. In the present study, special precautions have been taken so that the top and bottom walls out of thin brass sheets and exposing them to large volume flow rates of water. The side walls are made of 12.5 mm thick perspex sheets and padded using thermocole insulation. To avoid temperature tanks containing hot and cold water. The upper wall is cooled to a temperature below the ambient value and convection is initiated in this part of the cavity. The heat transfer rates at the hot and cold walls are unequal during the transient process and approach each other at steady state. Since the active boundary in the present work is the cold upper wall, the heat transfer rates have been computed in this region.

Previous Next

The cavity used in the present work is 74 cm long, thus giving an aspect ratio of 15 to 20. As stated earlier, the resulting flow is expected to be in the form of cells with an axis parallel to the longer side. The light beam of the interferometer averages the temperature field along the length of the cavity. The temperatures of the hot and cold walls are measured using ten 18 gage chromel-alumel thermocouples on each surface. Temperature on each surface is found to be constant within $\pm 0.2^{\circ}C$ along the path of the light beam. The hot and the cold walls of the cavity reach steady state in about two hours. Environmental conditions in the laboratory are stable for three hours and data is colected over this duration.

At the Rayleigh numbers considered in the present investigation the fringes in the core of the cavity are not strictly stationary even after a sufficiently long time is allowed to elapse. To estimate the extent of this uncertainty in the heat transfer data the following procedure has been adopted. Five interferometric image are recorded at the camera snapping speed of one picture every 20 minutes at predetermined instants of time. This time interval is requied to transfer light intensity data over 512×512 pixels from the camera to the PC. The Nusselt number evaluated at 20 minute intervals. The uncertainty in this average Nusselt number in relation value is as $\pm 20\%$ with 95% high as with confidence.

The time required to collect five images consecutively is 100 minutes. This time is, however, small in comparison to the time scale of evolution of flow. The first image is typically collected after 8 to 10 minutes and the flow reaches steady state after 2 to 3 hours. Hence, the response time of the measurement system can be considered to be negligible.

Previous